

Thermalization time and specific heat of the neutron stars crust

M. Fortin,^{1,2} F. Grill,³ J. Margueron,¹ Dany Page,⁴ and N. Sandulescu^{5,*}

¹*Institut de Physique Nucléaire, IN2P3-CNRS, and Université Paris-Sud, F-91406 Orsay Cedex, France*

²*École Normale Supérieure, Département de Physique, 24 rue Lhomond, F-75005 Paris, France*

³*Dipartimento di Fisica, Università degli Studi di Milano, Via Celoria 16, I-20133 Milan, Italy*

⁴*Departamento de Astrofísica Teórica, Instituto de Astronomía, Universidad Nacional Autónoma de México, 04360 Mexico City Distrito Federal, Mexico*

⁵*National Institute of Physics and Nuclear Engineering, RO-76900 Bucharest, Romania*

(Received 28 October 2009; revised manuscript received 5 December 2010; published 27 December 2010)

We discuss the thermalization process of the neutron star's crust described by solving the heat-transport equation with a microscopic input for the specific heat of baryonic matter. The heat equation is solved with initial conditions specific to a rapid cooling of the core. To calculate the specific heat of inner-crust baryonic matter, that is, nuclear clusters and unbound neutrons, we use the quasiparticle spectrum provided by the Hartree-Fock-Bogoliubov approach at finite temperature. In this framework, we analyze the dependence of the crust thermalization on pairing properties and on cluster structure of inner-crust matter. It is shown that the pairing correlations reduce the crust thermalization time by a large fraction. The calculations show also that the nuclear clusters have a non-negligible influence on the time evolution of the surface temperature of the neutron star.

DOI: [10.1103/PhysRevC.82.065804](https://doi.org/10.1103/PhysRevC.82.065804)

PACS number(s): 26.60.Gj

I. INTRODUCTION

The thermalization process of the neutron star's crust can give important information concerning the properties of the crust matter. This is indeed the case in the cooling of isolated neutron stars [1] and in the thermal afterburst relaxation of neutron stars from x-ray transients [2,3]. In the rapid cooling process, an important quantity is the cooling or thermalization time of the crust, defined as the time needed for the crust matter to equilibrate its temperature to the temperature of the colder core. The outer crust, because of its thinness and the very small amount of matter it contains, has a very short thermal time scale. Hence, the cooling time is essentially determined by the inner-crust matter, formed by nuclear clusters, unbound neutrons, and ultrarelativistic electrons.

The thermalization time of the crust depends essentially on the crust thickness [1]. However, several studies have shown that the thermalization time depends also significantly on the superfluid properties of the inner-crust baryonic matter [1,4–7]. This dependence is induced through the specific heat of unbound neutrons, strongly affected by the pairing energy gap. Since the neutron-pairing gap is influenced by the presence of the nuclear clusters [5,8,9], a reliable calculation of neutron-specific heat should take the clusters into account. How the intensity of pairing correlations affects the specific heat of the neutrons in the presence of nuclear clusters was analyzed in Ref. [10]. Thus, using the framework of the Hartree-Fock-Bogoliubov (HFB) approach at finite temperature, it was shown that the specific heat can change with several orders of magnitude if the pairing gap is adjusted to describe two possible scenarios for neutron-matter superfluidity, that is, one corresponding to the BCS approximation and the other to calculation schemes that take into account in-medium

effects [11]. The impact that these changes in the specific heat could have on the thermalization time was discussed in Ref. [6]. By employing a simple random-walk model for the cooling [5,12], in which the diffusion of the heat toward the core was calculated without taking into account the dynamical change of the temperature through the whole crust, it was shown that the thermalization times corresponding to the two pairing scenarios mentioned previously differ by a large fraction. The scope of this paper is to present more accurate estimations of the thermalization time obtained by employing a more realistic cooling model based on dynamical solutions of the heat equations [13] and on a state-of-the-art description of the specific heat for baryonic matter.

II. THE MODEL OF CRUST THERMALIZATION

The crust thermalization is described here in the rapid cooling scenario in which the core arrives quickly at a much cooler temperature than the crust. Because of this temperature inversion, the heat stored in the crust diffuses into the core, where it is dissipated by the neutrinos. In addition, the crust cools also through direct neutrino emissivity processes. The heat diffusion can be described by the relativistic heat equation [14]

$$\frac{\partial}{\partial r} \left[\frac{Kr^2}{\Gamma(r)} e^\phi \frac{\partial}{\partial r} (e^\phi T) \right] = r^2 \Gamma(r) e^\phi \left(C_V \frac{\partial T}{\partial t} + e^\phi Q_\nu \right), \quad (1)$$

where T is the temperature, t is the time, K is the thermal conductivity, C_V is the specific heat, and Q_ν is the neutrino emissivity. The effect of the gravity is given through the gravitational potential ϕ , which enters in the definition of the red-shifted temperature $\tilde{T} = T e^\phi$, and the quantity $\Gamma(r) = (1 - 2Gm(r)/rc^2)^{-1/2}$, where G is the gravitational constant and $m(r)$ is the gravitational mass included in a sphere of radius r . The latter is obtained from the

* sandulescu@theory.nipne.ro

Tolman-Oppenheimer-Volkoff (TOV) equations. In this study, the properties of the neutron star are obtained by solving the TOV equations with an equation of state (EOS) based on a nuclear interaction of the Skyrme type, that is, SLy4 [15]. The details on this EOS are given in Ref. [16].

The cooling calculations presented here are for a neutron star of a mass equal to $1.6 M_{\odot}$. For this mass, the TOV equations predicts a total star radius of 11.49 km and a central density of $4.06 \rho_0$, where $\rho_0 = 2.9 \times 10^{14} \text{ g cm}^{-3}$ is the saturation density of symmetric nuclear matter. The inner crust, defined here as the part of the star with the density ranging between $\rho_{\text{core}} = 1.6 \times 10^{14} \text{ g cm}^{-3}$ and $\rho_{\text{drip}} = 4 \times 10^{11} \text{ g cm}^{-3}$, extends from $R_c = 10.72 \text{ km}$, which is the radius at the core-crust interface, to 11.19 km.

The cooling process is described by solving the heat equation (1) in the whole volume of the neutron star. The initial temperature distribution in the star is chosen to be constant, $T(r, t = 0) = T_i$. The three needed microphysical ingredients, K , C_V , and Q_V , as well as pairing of neutron and protons in the core, are described here, except for the crust C_V , which is considered in more detail in the next section.

For the neutrino emissivity of the core, we consider the contribution of the modified URCA and bremsstrahlung processes, and we impose the direct URCA fast-cooling process at densities $\rho > 0.5 \times 10^{15} \text{ g cm}^{-3}$. In the crust, we include neutrino emission by the plasmon decay, which is the dominant process at high temperature in the outer crust, as well as the electron-ion, electron-electron, and neutron-neutron bremsstrahlung processes. When neutron and/or protons become superfluid or superconducting, suppression of the neutrino processes in which they participate is taken into account and the Cooper pair breaking and formation (PBF) process is turned on. See, for example, Ref. [17] for a detailed presentation, and notice that we have taken into account the vector channel suppression in the PBF process [18].

Neutron and proton pairing in the core is taken into account using critical-temperature profiles from Ref. [19] for the proton 1S_0 gap and the model “a” of Ref. [20] for the neutron 3P_2 gap. Our model for the neutron 1S_0 pairing in the crust is described in the next section.

The thermal conductivity from a component “x” can, generically, be written as

$$K^x = \frac{C_V^x \langle v^x \rangle^2}{3\nu^x}, \quad (2)$$

where C_V^x is its specific heat, $\langle v^x \rangle$ is its velocity, and ν^x is its collisional frequency. For degenerate fermions, $\langle v^x \rangle = v_F^x$, the Fermi velocity. In the crust, we consider only the electron contribution, K^e , and apply Matthiessen’s rule to write $\nu^e = \nu^{e-\text{ion}} + \nu^{e-e}$. We follow the prescriptions of Ref. [4] to calculate the electron-ion collision frequency $\nu^{e-\text{ion}}$ and Ref. [21] for the electron-electron one, ν^{e-e} . Several factors may strongly affect the crust conductivity, but we neglect these effects because of the uncertainty inherent in them. For instance, there is a possible contribution coming from the electron-impurity scattering, $\nu^{e-\text{imp}}$, which would lower the conductivity at low temperatures, but this contribution depends on the unknown charge and density of impurities; there is also a contribution due to magnetic fields higher than

10^{13} G , which renders the electron conductivity anisotropic, but the effect is not taken into account because of the unknown internal geometry of the magnetic field; finally, the superfluid phonon conductivity, K^{sPh} , might also provide a significant contribution at high temperatures since $C_V^{\text{sPh}} \propto T^3$, but only crude estimates of their mean free path $\lambda^{\text{sPh}} = v^{\text{sPh}}/\nu^{\text{sPh}}$ exist.

In the core, we include the contribution of the leptons, K^e and K^μ [22], and nucleons, K^p and K^n [23]. The lepton contribution dominates and is strongly affected by the proton superconductivity. Electromagnetic scattering through longitudinal photons (“Coulomb” or “electric” scattering) is always screened (Debye screening) and is hence a short-range interaction. However, scattering through transverse photons (“magnetic” scattering) in a normal plasma is only moderated by Landau damping: for relativistic particles, as e and possibly μ are, this results in large scattering rates. Once the protons are superconductors, transverse photons are screened (Meissner screening) and the whole electromagnetic scattering becomes short range. Consequently, in the presence of proton superconductivity, K^e and K^μ exhibit the typical behavior of a Fermi liquid, being $\propto T^{-1}$, while when protons are normal, K^e is independent of T [24]. The overall dependence of K on density is shown in Fig. 1 for three temperatures, that is, $T = \{10^7, 10^8, 10^9\} \text{ K}$, typical for the cooling calculations performed in this study. In the crust, the conductivity shown in Fig. 1 is similar to that of Ref. [4]. In the core, Fig. 1 clearly exhibits the $\propto T^{-1}$ behavior at densities $\rho < 5 \times 10^{14} \text{ g cm}^{-3}$ where protons are superconductors, in contrast to the T -independent values at higher densities. This high-density behavior of K^e was absent in the work of Ref. [4], which came before Ref. [22].

To solve the heat equations in the whole volume of the neutron star, we need the specific heat in the core and crust regions. The dependence of the specific heat on the density is illustrated in Fig. 2 for a temperature equal to 10^9 K . In the outer crust, the specific heat has contributions from the electrons and the ions, while in the core it has contributions from electrons, the neutrons, and the protons. These specific

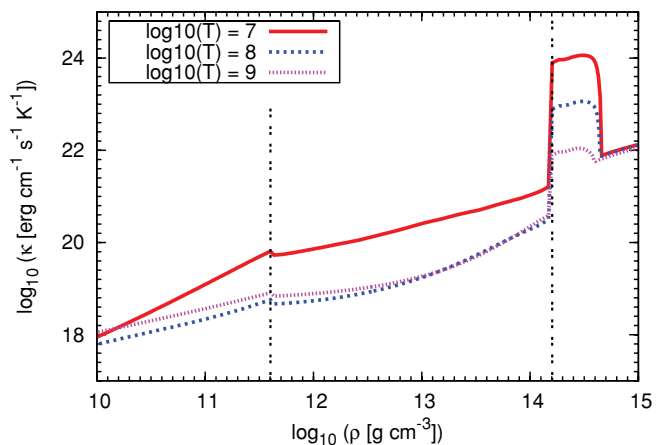


FIG. 1. (Color online) The total conductivity in the neutron star as a function of the density and for the temperatures $T = \{10^7, 10^8, 10^9\} \text{ K}$ (see the text for more details). The bounds of the inner crust are indicated by the vertical lines.

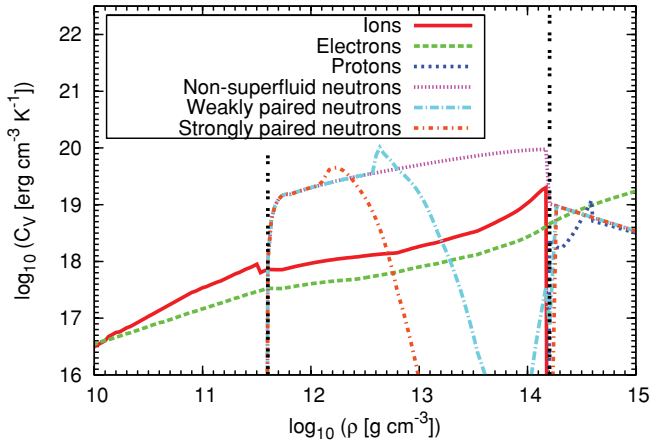


FIG. 2. (Color online) Specific heat in the crust of the neutron star for the different components of the star matter and for a temperature of 10^9 K (see the text for more details).

heats are evaluated using standard approximations (see, e.g., [20]). The specific heat of the nonuniform inner-crust matter is discussed in the next section.

III. SPECIFIC HEAT OF THE INNER-CRUST MATTER

The specific heat of the inner crust has contributions from the electrons, the lattice, and the unbound neutrons. They are calculated for a given set of densities in the Wigner-Seitz approach. Since the electrons are ultrarelativistic, they are considered as a uniform degenerate gas with the specific heat given by [25]

$$C_V^{(e)} = \frac{k_B(3\pi)^{2/3}}{3\hbar c} \left(\frac{Z}{V}\right)^{2/3} T, \quad (3)$$

where V is the volume of the Wigner-Seitz cell and Z is the number of the electrons in the cell (which is equal to the number of protons).

The thermodynamic state of the ions is determined by the Coulomb coupling parameter

$$\Gamma = \frac{(Ze)^2}{ak_B T}, \quad (4)$$

where a is the radius of the Wigner-Seitz cell. Monte-Carlo simulations of the one-component plasma (OCP) show that crystallization occurs at $\Gamma \simeq 175$, but supercooling can occur and push the phase transition to higher values of Γ . For the specific heat of the nuclei, we use the OCP results of Ref. [26] in the liquid phase while in the solid phase we include the harmonic crystal results of Ref. [27] complemented by a small anharmonic correction following the recipe proposed in Ref. [28]. In the liquid at high Γ and in the classical solid, the specific heat per ion is $\sim 3k_B$. With lowering temperature, quantum effects set in and, in the asymptotic limit of very low T , one obtains the Debye result

$$C_V = n_i \cdot \frac{12\pi^4}{5} \left(\frac{T}{\Theta_D}\right)^3, \quad (5)$$

where the Debye temperature, Θ_D , is related to the ion plasma temperature, T_P , by

$$\Theta_D = \alpha T_P, \quad T_P \equiv \frac{\hbar}{k_B} \left(\frac{4\pi(Ze)^2 n_i}{m_i}\right)^{1/2}, \quad (6)$$

where m_i is the ion mass. For a Coulomb crystal, as is the case in a neutron star crust, $\alpha \simeq 0.45$ [29], and the Debye regime [Eq. (5)] is reached when $T \leq 0.1T_P$.

We now discuss the temperature dependence of the specific heat of neutrons, which requires more elaborate calculations. In the inner crust, the unbound neutrons are superfluid in the 1S_0 channel. To take into account the superfluid properties of the neutrons as well as the nonuniform cluster structure of the inner crust, we perform HFB calculations at finite-temperature for each Wigner-Seitz cell shown in the table in Appendix A. The details of the HFB calculations in a Wigner-Seitz cell are given in Ref. [10]. In the HFB calculations, the mean field is described with the same interaction used in the star model, that is, the Skyrme force SLy4. A completely consistent cooling simulation would require Wigner-Seitz cells determined with the same Skyrme interaction and using the framework of the temperature-dependent HFB approach. In this way, one could take into account the effects of pairing and temperature on the inner-crust structure. Since at present there are not such self-consistent HFB calculations for the inner-crust structure, here we use the Wigner-Seitz cells of Ref. [30]. Their structure, determined in the Hartree-Fock approach and with a Skyrme-like effective interaction obtained from the density matrix expansion approximation, are summarized in the table in Appendix A. As seen there, the cells have magic and semimagic numbers of protons. This indicates that the proton spin-orbit interaction has an important effect on the structure of Wigner-Seitz cells. This effect is not taken into account in the inner-crust structure calculations based on the liquid-drop model [16].

The pairing correlations in the inner-crust matter are described with a density-dependent contact force of the following form [31]:

$$V(\mathbf{r} - \mathbf{r}') = V_0 \left[1 - \eta \left(\frac{\rho(r)}{\rho_0}\right)^\alpha\right] \delta(\mathbf{r} - \mathbf{r}'), \quad (7)$$

where $\rho(r)$ is the baryonic density. To analyze the dependence of the crust thermalization on the intensity of pairing correlations, in the calculations we have used two sets of parameters for the pairing force. They are chosen to simulate two possible scenarios for pairing in neutron matter corresponding to (1) BCS calculations with realistic two-body interactions extracted from nucleon-nucleon scattering [11] (in this approximation, the maximum pairing gap in uniform neutron matter is about 3 MeV); and (2) calculations that go beyond the BCS approximation by taking into account in-medium effects on two-body interaction and self-energy (these calculations predicts a maximum pairing gap in neutron matter of about 1 to 1.5 MeV [32,33]). Two similar scenarios,

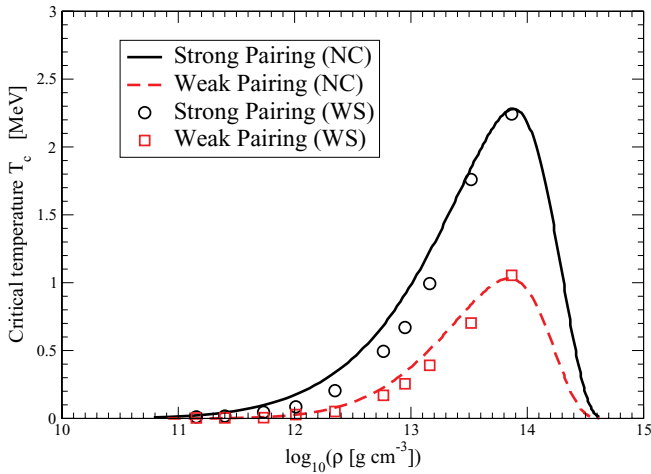


FIG. 3. (Color online) Critical temperature corresponding to the weak and strong pairing force obtained solving the BCS equations in uniform neutron matter (NC). The critical temperatures labeled (WS) are obtained by the relation $T_c = 0.567\Delta_0$, where Δ_0 is the average pairing field in the neutron gas region at $T = 0$ calculated in the HFB approach and Wigner-Seitz approximation.

called strong and weak pairing, are simulated by using two pairing forces with the same parameters for the density-dependent part, namely $\eta = 0.7$ and $\alpha = 0.45$, and two different strengths, that is, $V_0 = \{-570, -430\} \text{ MeV fm}^{-3}$. These parameters have been used with an energy cutoff in the quasiparticle spectrum, required by the zero range of the pairing force. The cutoff was introduced smoothly, that is, by an exponential factor $\exp(-E_i^2/100)$ acting for $E_i > 20 \text{ MeV}$, where E_i are the HFB quasiparticle energies. The smooth cutoff was introduced in order to reduce the numerical fluctuations generated in the self-consistent HFB calculations by the discretization of the continuum quasiparticle spectrum. The critical temperatures in uniform matter obtained with these two pairing interactions and using the same cutoff prescription as in the HFB calculations are shown in Fig. 3. The same figure also shows the critical temperatures obtained by the relation $T_c = 0.567\Delta_0$ (see Appendix C), where Δ_0 is the average pairing field in the neutron gas region at $T = 0$ calculated in the HFB approach and Wigner-Seitz approximation. It can be noticed that these critical temperatures are rather close to the ones obtained for the uniform matter.

With the setting discussed previously, we have solved the HFB equations for a given Wigner-Seitz cell and determined the quasiparticle spectrum E_i and the corresponding entropy, that is,

$$S = -k_B \sum_i (2j_i + 1) [f_i \ln f_i + (1 - f_i) \ln(1 - f_i)], \quad (8)$$

where $f_i = [1 + \exp(E_i/k_B T)]^{-1}$ is the Fermi distribution. From the entropy, we then calculated the specific heat of the neutrons

$$C_V = \frac{T}{V} \frac{\partial S}{\partial T}, \quad (9)$$

where V is the volume of the Wigner-Seitz cell.

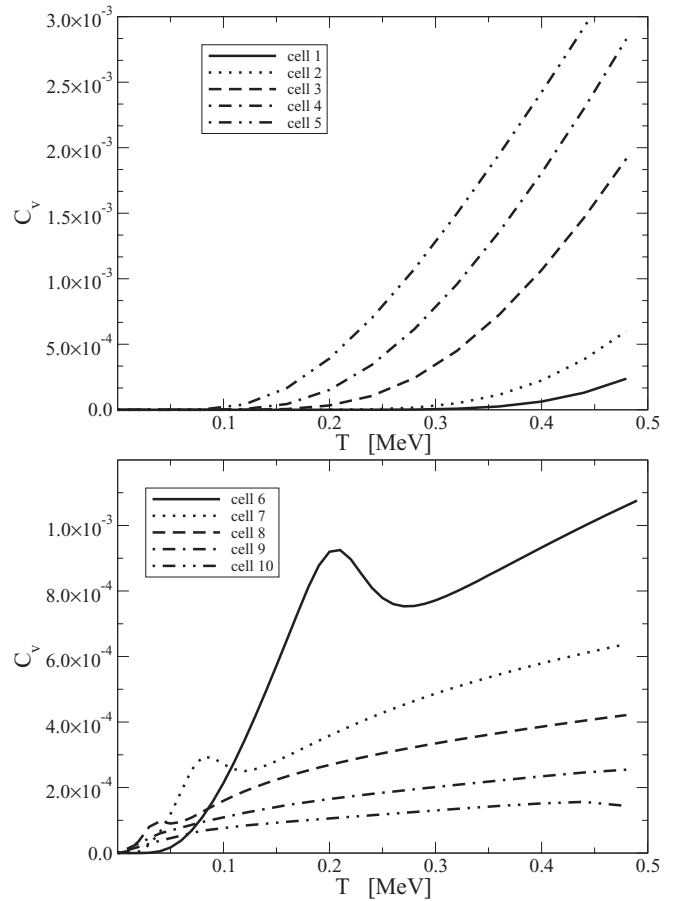


FIG. 4. Neutron-specific heats in various Wigner-Seitz cells for strong pairing. The specific heat is given in units of Boltzman constant k_B .

The specific heat was calculated for all cells listed in the table in Appendix A and for a set of temperatures covered by the thermalization process. These results have been used afterward for obtaining a parametrization of the specific heat in terms of temperature and density. The parametrization procedure is presented in Appendix C. The temperature dependence of the specific heat for the two scenarios of the pairing intensity is shown in Figs. 4 and 5. As discussed in Ref. [10], the specific heat has very different values for the two pairing scenarios. It is also interesting to notice that the specific heats of the cells have different temperature dependences. Thus, for the strong pairing scenario, shown in Fig. 4, the specific heat is in the superfluid regime for the first five cells (upper panel). This is not the case for the next cells (bottom panel) where in the same temperature range there is a transition from the superfluid to the normal phase, as clearly seen for cells 6–8. (For the last two cells, the transition temperature cannot be noticed because it is too small.) On the other hand, as seen in Fig. 5, for the weak pairing the specific heat is entirely in the superfluid regime only for the first two cells.

To illustrate the particular behavior of the specific heat in nonuniform matter and the validity of various approximations, in what follows we discuss in more detail the results for cell 6, which contains $N = 460$ neutrons and $Z = 40$ protons (see Appendix A). In this cell, the HFB calculations predict

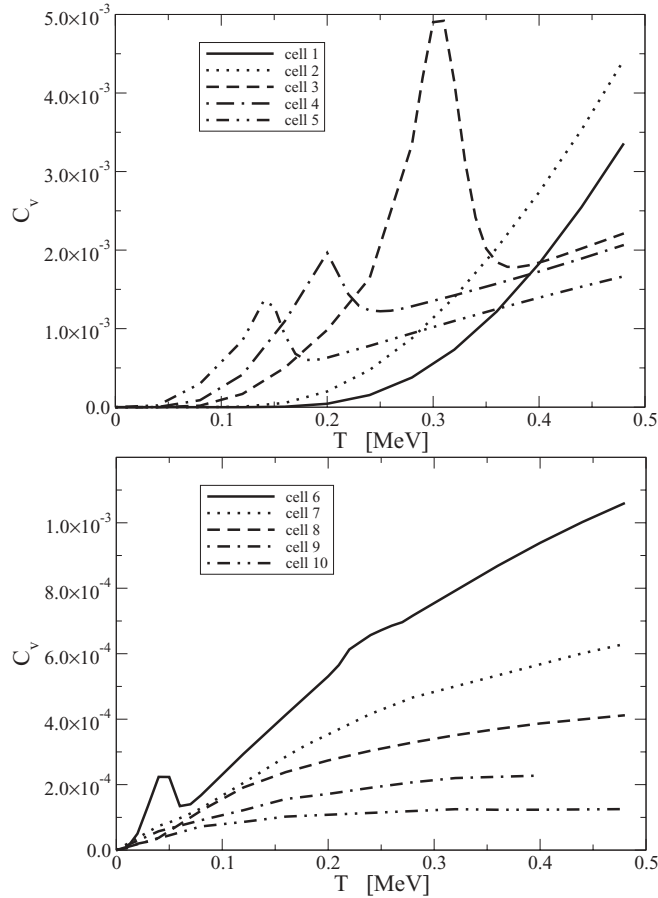


FIG. 5. Neutron-specific heats in various Wigner-Seitz cells for weak pairing. The specific heat is given in units of Boltzmann constant k_B .

378 unbound neutrons. It is interesting that in spite of many neutrons in the cell, the number of the bound neutrons in the cluster with $Z = 40$ protons is equal to the magic number 82, as for the dripline nucleus ^{122}Zr (see, e.g., Ref. [34]). The specific heat given by the HFB spectrum, in which the contribution of the cluster is included, is shown in Fig. 6 by a full line. The same figure also shows the specific heats corresponding to two approximations employed in some studies [1,5]. In these approximations, the nonuniform distribution of the neutrons is replaced with a uniform gas formed by the total number of neutrons in the cell (dashed line) or by taking only the number of the unbound neutrons (dash-dotted line). The latter case is considered an effective way of taking into account the influence of the cluster [5]. Figure 6 shows how these approximations work. To make the comparison meaningful, the calculations for the uniform neutron gas are done by solving the HFB equations with the same boundary conditions as for the nonuniform system, that is, neutrons plus cluster. As seen in Fig. 6, the transition from the superfluid to the normal phase takes place at a lower temperature in the case of uniform neutron gas, especially when only the unbound neutrons are considered. We can also notice that, in contrast to the uniform system, in the nonuniform system the transition from the superfluid to the normal phase is smooth.

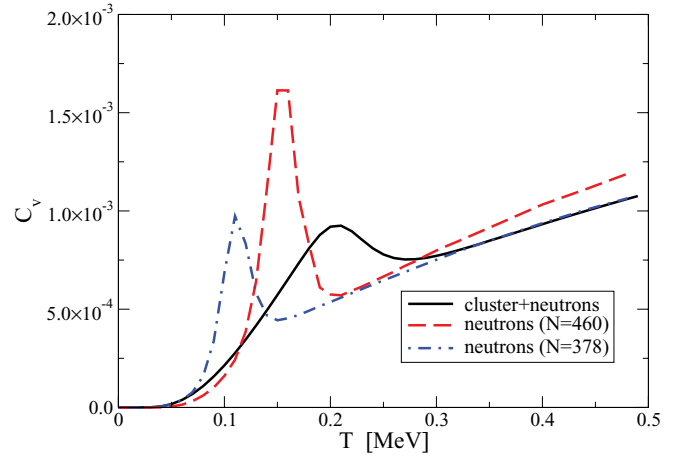


FIG. 6. (Color online) Neutron-specific heat in the Wigner-Seitz cell 6 for strong pairing. The results corresponds to various approximations discussed in the paper. The specific heat is given in units of Boltzmann constant k_B .

To see better what happens in a nonuniform system, Fig. 7 shows the evolution with the temperature of the pairing field in cell 6. The pairing field is defined by

$$\Delta(r) = V_0 \left[1 - \eta \left(\frac{\rho(r)}{\rho_0} \right)^\alpha \right] \kappa(r), \quad (10)$$

where $\kappa(r)$ is the local pairing tensor. To keep the analogy with the mean field, the pairing field is taken with negative values.

From Fig. 7, we can see that at zero temperature the pairing field is much larger at the surface of the cluster than in the bulk region. Because of this, by increasing the temperature, the pairs corresponding to the neutrons localized preferentially at the surface region of the cluster are destroyed gradually and much more slowly compared to the pairs formed by neutrons localized far from the surface of the cluster. In fact, as shown in Fig. 8, the nonuniform system shows two transition

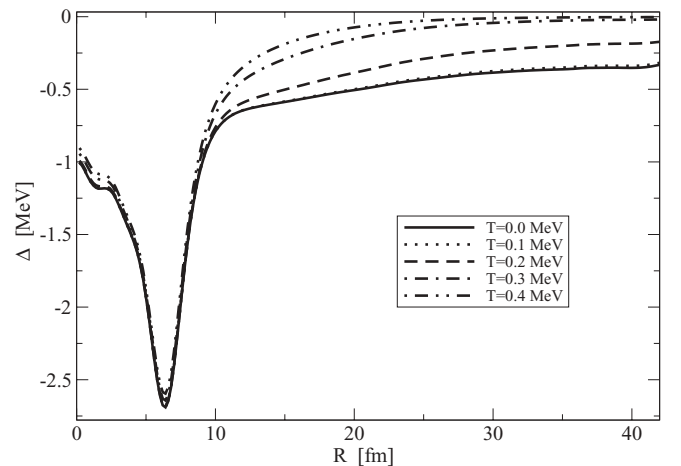


FIG. 7. Radial distribution of the pairing field for the Wigner-Seitz cell 6 for various temperatures. The results correspond to a strong pairing.

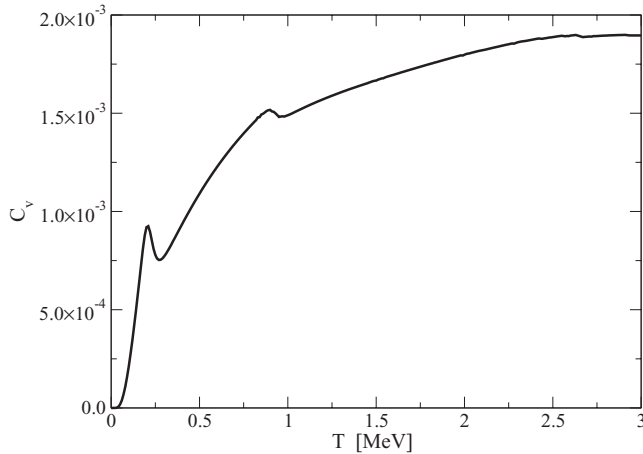


FIG. 8. Neutron-specific heat in the Wigner-Seitz cell 6 for strong pairing. Here the results are shown up to high temperatures in order to illustrate the second transition region around $T = 900$ keV. The specific heat is given in units of k_B .

regions, one around $T = 200$ keV, corresponding mainly to the neutrons located far from the surface of the cluster, and another one, much less pronounced, around $T = 900$ keV, which corresponds to the neutrons localized in the surface region of the cluster.

IV. CRUST THERMALIZATION

In this section, we discuss the crust thermalization obtained by solving the heat equation (1) with the specific heats presented in the previous sections. The time evolution of the temperature in the crust region is illustrated in Fig. 9. These results correspond to an initial temperature of $T_i = 500$ keV. To understand better the main effects that influence the thermalization, the results are shown separately for two time

intervals, that is, from $t = 10^{-5}$ yr up to 1 yr and from 1 to 15 yr.

In the first time interval, the star is too young for heat transport to play a significant role. Therefore $\partial T/\partial t \propto Q_\nu/C_V$, which means that the evolution is essentially determined by the local energy loss, $Q_\nu(r)$, and the local thermal inertia, $C_V(r)$. The effect of neutron pairing on the neutrino emission is moderate because it affects only the neutron-neutron bremsstrahlung and not the plasmon decay, the electron-ion, and electron-electron bremsstrahlung processes. However, the specific heat is strongly dependent on the physical state of the neutrons in the inner crust. Indeed, the pairing is strongly suppressing the contribution of the neutrons to the specific heat, which otherwise would give a dominant contribution; see, for instance, Fig. 2. In the region where neutrons are paired, the ions provide the major contribution to the specific heat, eventually being supplanted by the electrons since $C_V^{(\text{ion})} \propto T^3$ while $C_V^{(e)} \propto T$. The effects of these different regimes of specific heat are clearly seen from Fig. 9. Thus in the time interval from 10^{-4} to 10^{-1} yr, it can be seen that in the region where pairing is active, going from the crust-core boundary (at $r \sim 10.75$ km) up to $r \sim 11.15$ km in the case of strong pairing (upper right panel) or $r \sim 11.05$ km in the case of weak pairing (upper central panel), the cooling is much faster comparing to the case of no pairing (upper left panel). At the end of this first time interval, at age $\sim 10^{-1}$ yr, the temperature profile gradually becomes smoother as a result of transport of heat between neighboring layers. As a consequence, at about 1 yr the temperature profiles for the three pairing scenarios (i.e., no pairing, weak pairing, and strong pairing) become similar.

In the second interval of time, the intensity of pairing correlations influences significantly the thermal relaxation of the inner crust. As seen in Fig. 9, the cooling is much faster when the intensity of pairing correlations is stronger. In the time interval, the heat transport is the dominant factor in the thermal evolution of the crust, neutrino emission being mostly

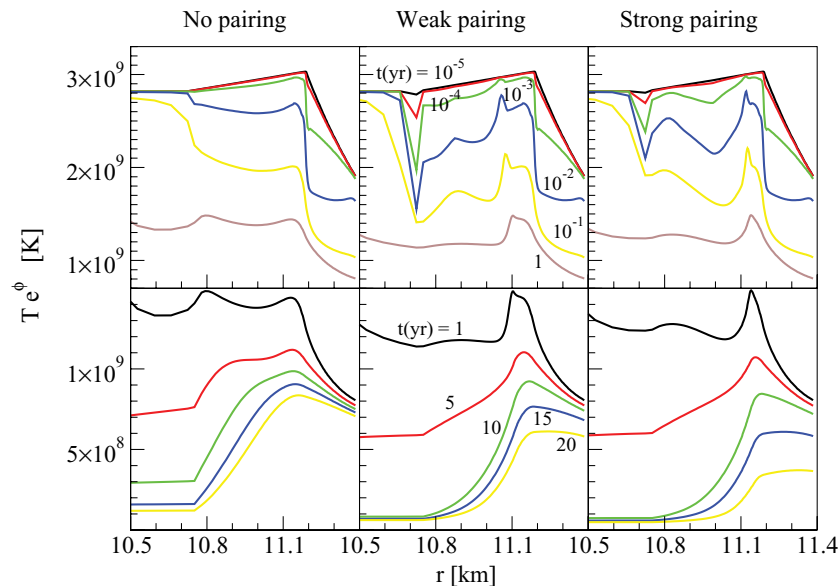


FIG. 9. (Color online) Time evolution of the red-shifted temperature T_e^ϕ inside the inner crust for $T_i = 500$ keV. The variable r represents the radius of the star in kilometers. The core-crust transition occurs at $r = 10.75$ km (see the text for more details).

due to the inefficient electron-ion bremsstrahlung process. The transport time scale is determined by the thermal conductivity K and the specific heat C_V through the ratio K/C_V , and the strong influence of pairing on cooling observed in the second time interval is induced by the effect that pairing has on the specific heat of neutrons.

The time evolution of the effective surface temperature T_∞^{eff} is displayed in Fig. 10 for two initial temperatures of the crust, $T_i = \{300, 500\}$ keV. The effective surface temperature shown in Fig. 10 is obtained from the temperature at the bottom of the crust, $T_b = T(\rho_b)$, where $\rho_b = 10^{10}$ g cm $^{-3}$, using the relationship given in Ref. [35] for a nonaccreted envelope. It can be seen that the time evolution of the surface temperature does not depend much on the initial temperature of the crust. As expected from the results shown in Fig. 9, the pairing significantly enhances the cooling at the surface of the star. The same conclusion was obtained previously in a random walk cooling model [6]. However, the latter predicts different thermalization times compared to the realistic cooling model employed here.

Figure 10 also shows the apparent surface temperatures obtained neglecting the effect of the clusters, that is, supposing

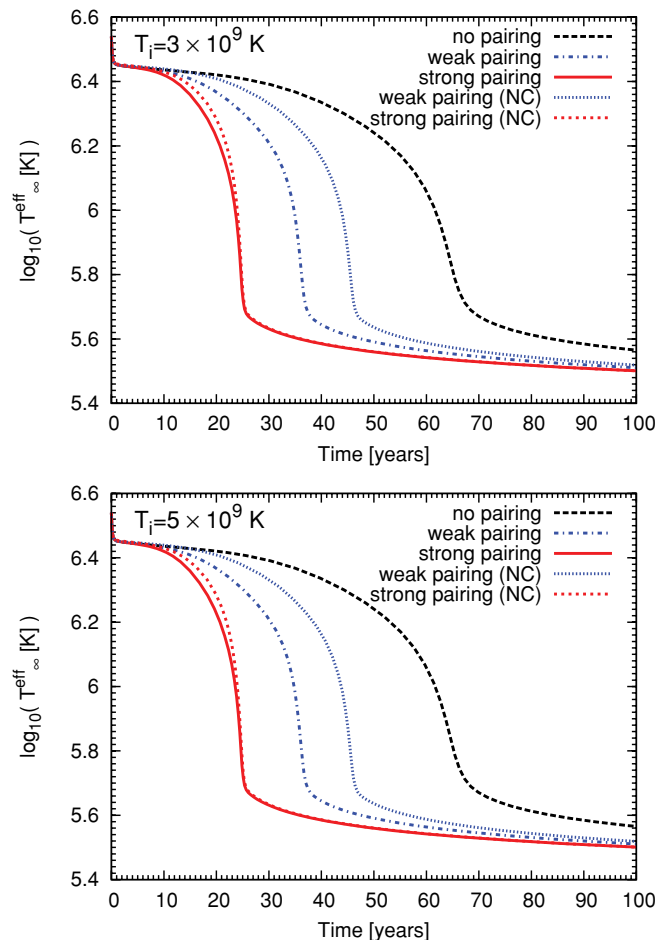


FIG. 10. (Color online) Time evolution of the apparent surface temperature for the initial temperatures $T_i = \{300, 500\}$ keV. NC indicates the results of the calculations obtained by neglecting the effect of the clusters.

that the neutron specific heat is given solely by that of the neutron gas. In this case, the specific heat of the neutrons is calculated from the quasiparticle spectrum of BCS equations solved for infinite neutron matter at a density corresponding to that of the external neutrons in the Wigner-Seitz cell [36]. It can be seen that for the weak pairing scenario the clusters have a non-negligible effect on the time evolution of the surface temperature.

The thermalization of the crust is commonly characterized by the cooling time t_w defined as the time for which the slope of the apparent surface temperature $T_\infty^{\text{eff}}(t)$ is larger in absolute value. In Refs. [1,4], it has been shown that the cooling time t_w scales with the parameter α defined as

$$\alpha = \left(\frac{\Delta R_{\text{crust}}}{1 \text{ km}} \right)^2 (1 - r_g/R)^{-3/2}. \quad (11)$$

It can be seen that the scaling parameter α depends solely on the global properties of the neutron star, that is, the crust thickness ΔR_{crust} , the star radius R , and the gravitational radius $r_g = 2GM/c^2$ where M is the mass of the star. To probe this scaling relation, we have estimated the cooling time for various neutron stars with masses between $1.4M_\odot$ and $2.0M_\odot$ with a step of $0.1M_\odot$ and for three different superfluid scenarios (normal neutrons, neutrons with weak pairing, and neutrons with strong pairing). The results, calculated for an initial temperature $T_i = 500$ keV, are shown in Fig. 11. This figure displays two sets of fits for t_w versus α , that is, a linear fit (dashed line) and a fit with a fractional power in the scaling parameter (solid line). Parameters of the fitting curves are given in Fig. 11. It can be noticed that the best fit is obtained with a fractional power in the scaling parameter, which is equal to 0.86 for the normal neutrons, 0.85 for weakly paired neutrons, and 0.89 for strongly paired neutrons. Considering the simpler linear fit (i.e., $t_w \approx \alpha t_1$), as done in

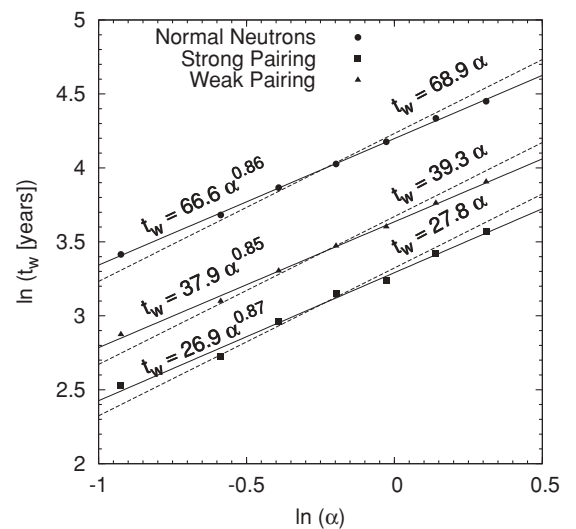


FIG. 11. Cooling times t_w vs scaling parameter α for three pairing scenarios as discussed in the text. The results correspond to neutron stars with masses between $1.4M_\odot$ and $2.0M_\odot$. The fitting curves are given for the case of a linear scale (dashed lines, right side) and for a fractional power of the scaling parameter α (solid lines, left side).

TABLE I. Cooling times t_w and normalized times t_1 for the linear scaling (see text for details). The results correspond to a neutron star of a mass equal to $1.5M_\odot$ and to three models for the neutron superfluidity in the inner crust.

| Model of neutron superfluidity | t_w | t_1 |
|--------------------------------|-------|-------|
| No superfluidity | 76.3 | 66.4 |
| Weak pairing | 43.1 | 37.4 |
| Strong pairing | 30.6 | 26.6 |

Refs. [1,4], we get for the normalized time t_1 the values $t_1 = \{68.9, 39.3, 22.3\}$ corresponding, respectively, to the normal neutrons, neutrons with weak pairing, and neutrons with strong pairing.

Table I gives the values of the cooling time t_w and the normalized time t_1 obtained for a $1.5M_\odot$ neutron star for which $\alpha = 1.15$. Compared to the results given in Table II of Ref. [4], our cooling calculations gives t_1 values that are larger by a factor 2.3 in the nonsuperfluid case and by 3.4 (3.0) for the weak (strong) pairing scenario. These differences could be explained by the effects of the nuclear clusters on the neutron specific heat, disregarded in Ref. [4], and by different neutrino processes and thermal conductivities in the core matter used in the two calculations.

V. SUMMARY AND CONCLUSIONS

In this paper, we have studied how the thermalization of a neutron star's crust depends on pairing properties and the cluster structure of the inner-crust matter. The thermal evolution was obtained by solving the relativistic heat equation with initial conditions specific to a rapid cooling process. The specific heat of neutrons was calculated from the HFB spectrum, taking into account the effects of nuclear clusters, pairing correlations, and temperature. The thermal evolution of the inner crust was analyzed using for the neutrons two sets of specific heat values obtained with strong and a weak pairing forces, which simulate two possible scenarios for the intensity of pairing correlations in neutron matter. The results show that the crust thermalization is strongly influenced by the intensity of pairing correlation. This result confirms those of Ref. [6] with a schematic cooling model. However, the latter predicts thermalization times that are different from the results obtained with the realistic cooling model employed in this study. We have also shown that the cluster structure of the inner crust significantly affects the time evolution of the surface temperature.

ACKNOWLEDGMENTS

We thank P. M. Pizzochero for valuable discussions. This work was supported by the European Science Foundation through the New Physics of Compact Stars project, by the Romanian Ministry of Research and Education through the CNCSIS Grant IDEI No. 270, and by ANR NExEN. D.P. acknowledges financial support through Grant IN122609 from DGAPA-Universidad Nacional Autonoma de Mexico.

TABLE II. The structure of the cells determined in Ref. [30], that is, the baryonic densities (ρ), the number of neutrons (N), the number of protons (Z), and the cell radii (R_{WS}). The last column shows the average densities in the neutron gas region provided by the present HFB calculations.

| Cell | N | Z | R_{WS} (fm) | ρ (g cm ⁻³) | $\tilde{\rho}_G$ (fm ⁻³) |
|------|------|----|------------------|---------------------------------|---|
| 10 | 140 | 40 | 54 | 4.7×10^{11} | 7.4×10^{-5} |
| 9 | 160 | 40 | 49 | 6.7×10^{11} | 1.3×10^{-4} |
| 8 | 210 | 40 | 46 | 1.0×10^{12} | 2.8×10^{-4} |
| 7 | 280 | 40 | 44 | 1.5×10^{12} | 5.3×10^{-4} |
| 6 | 460 | 40 | 42 | 2.7×10^{12} | 1.15×10^{-3} |
| 5 | 900 | 50 | 39 | 6.2×10^{12} | 3.0×10^{-3} |
| 4 | 1050 | 50 | 36 | 9.7×10^{12} | 4.6×10^{-3} |
| 3 | 1300 | 50 | 33 | 1.5×10^{13} | 7.5×10^{-3} |
| 2 | 1750 | 50 | 28 | 3.4×10^{13} | 1.7×10^{-2} |
| 1 | 1460 | 40 | 20 | 8.0×10^{13} | 3.8×10^{-2} |

APPENDIX A: THE STRUCTURE OF WIGNER-SEITZ CELL

This appendix summarizes the properties of the Wigner-Seitz cells determined in Ref. [30] and used in this paper. In contrast to Ref. [30], we do not shown the highest density cell. This cell is at the transition region to the more complicated pasta phases, and therefore its properties are believed to depend significantly on the model used to calculate the inner-crust structure. Table II shows the average densities in the neutron gas region, $\tilde{\rho}_G$, obtained in the present HFB calculations. These densities we have used for calculating the cooling curves in the no clusters (NC) approximation shown in Fig. 10.

APPENDIX B: CRUST THERMALIZATION IN A SIMPLE COOLING MODEL

The impact of the pairing correlations on the crust cooling can be analyzed in a simpler cooling model than the one employed in Sec. II. Here we present a model based on two simplifying assumptions. Thus, we suppose that the effect of the core on the crust cooling can be estimated through boundary and initial temperature conditions at the interface between the core and the crust. As shown in Ref. [1], this procedure works reasonably well in the case of a rapid cooling scenario. The second assumption is related to the neutrino emissivity of the crust. As shown in Fig. 8, the pairing is affecting the surface temperature at a later time of the thermalization process, of the order of 1 yr. Since after this time the neutrino emissivity of the crust becomes small, its contribution could be neglected when we analyze the influence of pairing intensity on crust cooling. Thus, considering the two assumptions discussed previously, the heat equation (1) is solved only in the region of the inner crust and neglects the neutrino emissivity.

Next, we discuss the initial and boundary conditions that simulate a rapid cooling of the core. The initial temperature distribution in the crust is chosen to be flat, $T(r, t = 0) = T_i$. At the interface between the core and the crust, we impose the

condition

$$\frac{\partial T(r = R_c, t)}{\partial t} = -\frac{e^{\phi(R_c)} Q_v}{C_V}. \quad (\text{B1})$$

Considering that the neutrino emissivity in the core is given by $Q_v = Q_f T_9^6$ [37], where $T_9 = T/10^9$ K, we obtain

$$T(r = R_c, t) = T_i (1 + \epsilon T_i^5 t)^{-1/5}$$

with

$$\epsilon = \frac{5e^{\phi(R_c)} Q_f}{C_V}. \quad (\text{B2})$$

For the constant Q_f , characterizing the fast neutrino emission in the core matter, we have taken the value $Q_f = 10^{26}$ erg cm⁻³ s⁻¹ [37].

In addition to these conditions, we have also considered that at the outer border of the crust the gradient of the temperature vanishes and at the bottom of the crust the temperature is given by the relationship given in Ref. [35] for a nonaccreted envelope.

In order to keep the calculations as simple as possible and to show that the conclusions about the effect of pairing on crust thermalization do not depend much on the level of approximation used for thermal conductivity and specific heat of the lattice, we have solved the heat equations with a different input than the calculations presented in Sec. II. Thus, for the thermal conductivity of the inner crust, we have used the parametrization given by Lattimer *et al.* [1], obtained from the calculations of Itoh *et al.* [38]. For temperatures above 10⁸ K, as used in this paper, the conductivity is nearly independent of the temperature and is given by $K = C(\rho/\rho_0)^{2/3}$, where $C = 10^{21}$ ergs cm⁻¹ s⁻¹ and ρ is the baryonic density.

For the specific heat of the neutrons and electrons, we have used the same input as in the complete cooling calculations. Since we are interested in analyzing only the relative values of cooling time corresponding to the two pairing scenarios, for the specific heat of the lattice we have taken the simplest approximation, that is, $C_V^{\text{lattice}} = 3k_B/V$, where V is the volume of the cell and k_B is the Boltzmann constant.

The time evolution of the apparent surface temperature obtained with the cooling model and the input discussed previously is shown in Fig. 12. It can be seen that these results and the ones presented in Fig. 9 have similar features relative to the effect of pairing on cooling. However, because of the crudeness of the simplifying approximations, the cooling times predicted by the cooling model employed in this section are smaller by a factor of 2 than the ones given by the realistic cooling calculations.

APPENDIX C: PARAMETRIZATION OF THE NEUTRON SPECIFIC HEAT IN THE INNER CRUST

In this appendix, we present the fitting procedure we have used to interpolate the specific heat of neutrons obtained from the HFB spectrum. The dependence of the specific heat on temperature and density is parametrized in the following form:

$$C_V^n = x_{\text{cl}} R C_V^q + (1 - x_{\text{cl}}) C_V^{\text{cl}}, \quad (\text{C1})$$

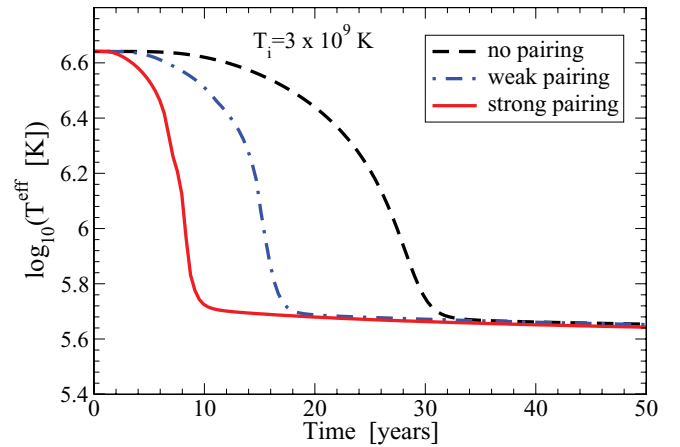


FIG. 12. (Color online) Time evolution of the surface temperature for the initial temperature $T_i = 300$ keV in the simple cooling model.

where R and x_{cl} are fitting functions, C_V^q is the specific heat of the unbound neutrons in the nonsuperfluid phase, and C_V^{cl} is its classical limit. The specific heat of nonsuperfluid neutrons in the quantum regime is expressed at low temperature as

$$C_V^q(T, \rho_n, N, R_{\text{WS}}) = \frac{1}{6} \left(\frac{2m_n^*}{\hbar^2} \right)^{3/2} \varepsilon_F^{1/2} T \left[1 - \frac{7}{40} \left(\frac{\pi T}{\varepsilon_F} \right)^2 - \frac{155}{896} \left(\frac{\pi T}{\varepsilon_F} \right)^4 \right], \quad (\text{C2})$$

where m_n^* is the effective mass of the neutrons, which, in the present calculations, depends on the density according to the Skyrme interaction SLy4 [15], and $\varepsilon_F = \hbar^2 k_F^2 / 2m_n^*$ is the Fermi energy at zero temperature. Equation (C2), valid for $\varepsilon_F < T$, can be derived using the expressions given in Ref. [25].

The specific heat of neutrons reaches the classical limit in the low-density region of the inner crust and at high temperatures (see Figs. 3 and 4). More precisely, the classical limit of the quantum specific heat is obtained for $T \gg \varepsilon_F$ and has the expression

$$C_V^{\text{cl}}(T, \rho_n, N, R_{\text{WS}}) = \frac{3}{2} \rho_{\text{gas}}(T, N, R_{\text{WS}}, \rho_n), \quad (\text{C3})$$

where ρ_{gas} is the density of the neutron gas (outer region of the cell) at temperature T , N is the number of neutrons in the cell, R_{WS} is the radius of the Wigner-Seitz cell, and ρ_n is the density of the neutron gas at zero temperature. The density of the neutron gas at finite T is different from that at $T = 0$ because of the dripping of the neutrons from the cluster to the gas induced by the thermal excitations. For $T < T_{\text{gas}} = 5.5$ MeV, the neutron gas at finite temperature can be expressed in the following form:

$$\rho_{\text{gas}}(T, N, R_{\text{WS}}, \rho_n) = \rho_n(T = 0) + \frac{T}{T_{\text{gas}}} [\rho_{\text{max}}(N, R_{\text{WS}}) - \rho_n(T = 0)], \quad (\text{C4})$$

while for $T > T_{\text{gas}} = 5.5$ MeV

$$\rho_{\text{gas}}(T, N, R_{\text{WS}}, \rho_n) = \rho_{\text{max}}(N, R_{\text{WS}}), \quad (\text{C5})$$

TABLE III. The parameters (a_0, a_1, a_2, a_3) that define the fitting functions employed in Eq. (C1). They are determined from the fit with the specific heat obtained from the HFB calculations done with the weak and strong pairing forces. The last column gives also the pairing gaps in the gas region at zero temperature.

| Cell | Weak | | | | | Strong | | | | |
|------|-------|-------|-------|-------|------------------|--------|-------|-------|-------|------------------|
| | a_0 | a_1 | a_2 | a_3 | Δ_o (MeV) | a_0 | a_1 | a_2 | a_3 | Δ_o (MeV) |
| 10 | 0.567 | 1.0 | 1.0 | 0.001 | 0.00 | 0.5 | 1.0 | 1.0 | 0.005 | 0.02 |
| 9 | 0.567 | 1.0 | 1.0 | 0.001 | 0.01 | 0.5 | 1.0 | 1.0 | 0.005 | 0.03 |
| 8 | 0.567 | 1.0 | 1.0 | 0.001 | 0.01 | 0.5 | 1.0 | 1.0 | 0.005 | 0.08 |
| 7 | 0.567 | 1.1 | 1.1 | 0.001 | 0.05 | 0.567 | 1.0 | 1.0 | 0.015 | 0.15 |
| 6 | 0.4 | 1.4 | 1.4 | 0.001 | 0.09 | 0.567 | 1.1 | 1.1 | 0.025 | 0.36 |
| 5 | 0.567 | 0.9 | 0.78 | 0.005 | 0.30 | 0.60 | 1.0 | 1.0 | 0.025 | 0.87 |
| 4 | 0.567 | 0.83 | 0.75 | 0.01 | 0.45 | 0.62 | 1.0 | 1.0 | 0.025 | 1.18 |
| 3 | 0.567 | 0.84 | 0.7 | 0.01 | 0.69 | 0.567 | 0.97 | 0.91 | 0.02 | 1.75 |
| 2 | 0.567 | 0.89 | 0.8 | 0.01 | 1.24 | 0.53 | 0.93 | 0.86 | 0.015 | 3.10 |
| 1 | 0.567 | 0.84 | 0.72 | 0.01 | 1.86 | 0.54 | 0.935 | 0.88 | 0.015 | 3.95 |

where $\rho_{\max}(N, R_{\text{WS}})$ is the density obtained if all the neutrons are distributed uniformly in the cell and $\rho_n(T=0) = \bar{\rho}_G$ given in Table II.

The fitting function x_{cl} , related to the quantum and classical limit of the specific heat, is defined as

$$x_{\text{cl}} = \left(1 + e^{5\left(\frac{\pi T}{\epsilon_F} - 1\right)}\right)^{-1}. \quad (\text{C6})$$

In Eq. (C1), the function R simulates the reduction of the specific heat due to pairing correlations. For its expression, we take the following form:

$$R(T, N, R_{\text{WS}}, a_3) = R_{\text{YL}}(u) f_1(T, \Delta_o, a_0, a_1, a_3) + [1 - f_2(T, \Delta_o, a_0, a_2, a_3)], \quad (\text{C7})$$

where

$$R_{\text{YL}}(u) = (0.4186 + \sqrt{1.007^2 + (0.501u)^2})^{5/2} \times e^{1.456 - \sqrt{1.456^2 + u^2}}. \quad (\text{C8})$$

This expression is similar to the suppression factor employed in Ref. [36] for uniform neutron matter. The quantity u is a function of $x = T/T_C$ where T_C is the critical temperature associated with the superfluid- to normal-phase transition. For

$x < 1$, the function $u(x)$ is given by

$$u(x) = \sqrt{1-x} \left(1.456 - \frac{0.157}{\sqrt{x}} + \frac{1.764}{x}\right), \quad (\text{C9})$$

while for $x > 1$ the function is vanishing, that is, $u(x) = 0$.

The functions f_1 and f_2 are introduced to describe the smooth transition from the superfluid to the normal phase and are given by

$$f_1(T, \Delta_o, a_0, a_1, a_3) = \frac{(1 + e^{-a_1 a_0 \Delta_o / a_3})}{(1 + e^{(T - a_1 a_0 \Delta_o) / a_3})}, \quad (\text{C10})$$

$$f_2(T, \Delta_o, a_0, a_2, a_3) = \frac{(1 + e^{-a_2 a_0 \Delta_o / a_3})}{(1 + e^{(T - a_2 a_0 \Delta_o) / a_3})}. \quad (\text{C11})$$

The quantity Δ_0 is the pairing energy gap in the neutron gas at $T = 0$. Its value is related to the critical temperature by $T_C = a_0 \Delta_0$. The parameters (a_0, a_1, a_2, a_3) are adjusted to reproduce the specific heats calculated from the HFB spectrum. Their values are given in Table III for the weak and strong pairing scenarios.

- [1] J. M. Lattimer, K. A. Van Riper, M. Prakash, and M. Prakash, *Astrophys. J.* **425**, 802 (1994).
- [2] P. S. Shternin, D. G. Yakovlev, P. Haensel, and A. Y. Potekhin, *Mon. Not. R. Astron. Soc.* **382**, L43 (2007).
- [3] E. F. Brown and A. Cumming, *Astrophys. J.* **698**, 1020 (2009).
- [4] O. Y. Gnedin, D. G. Yakovlev, and A. Y. Potekhin, *Mon. Not. R. Astron. Soc.* **324**, 725 (2001).
- [5] P. M. Pizzochero, F. Barranco, E. Vigezzi, and R. A. Broglia, *Astrophys. J.* **569**, 381 (2002).
- [6] C. Monrozeau, J. Margueron, and N. Sandulescu, *Phys. Rev. C* **75**, 065807 (2007).
- [7] N. Sandulescu, *Eur. Phys. J. (Special Topics)* **156**, 265 (2008).
- [8] F. Barranco, R. A. Broglia, H. Esbensen, and E. Vigezzi, *Phys. Rev. C* **58**, 1257 (1998).
- [9] N. Sandulescu, N. V. Giai, and R. J. Liotta, *Phys. Rev. C* **69**, 045802 (2004).
- [10] N. Sandulescu, *Phys. Rev. C* **70**, 025801 (2004).
- [11] U. Lombardo, in *Nuclear Methods and the Nuclear Equation of State*, edited by M. Baldo (World Scientific, Singapore, 1999), pp. 458–510.
- [12] G. E. Brown, K. Kubodera, D. Page, and P. M. Pizzochero, *Phys. Rev. D* **37**, 2042 (1988).
- [13] D. Page, U. Geppert, and F. Weber, *Nucl. Phys. A* **777**, 497 (2006); D. Page and S. Reddy, *Ann. Rev. Nucl. Part. Sci.* **56**, 327 (2006).
- [14] K. S. Thorne, *Astrophys. J.* **212**, 825 (1977).
- [15] E. Chabanat, P. Bonche, P. Haensel, J. Meyer, and R. Schaeffer, *Nucl. Phys. A* **627**, 710 (1997).
- [16] F. Douchin and P. Haensel, *Astron. Astrophys.* **380**, 151 (2001).
- [17] D. G. Yakovlev, A. D. Kaminker, O. Y. Gnedin, and P. Haensel, *Phys. Rep.* **354**, 1 (2001).

- [18] L. B. Leinson and A. Perez, *Phys. Lett. B* **638**, 114 (2006).
- [19] T. Takatsuka, *Prog. Theor. Phys.* **50**, 1754 (1973).
- [20] D. Page, J. M. Lattimer, M. Prakash, and A. W. Steiner, *Astrophys. J. Suppl.* **155**, 623 (2004).
- [21] P. S. Shternin and D. G. Yakovlev, *Phys. Rev. D* **74**, 043004 (2006).
- [22] P. S. Shternin and D. G. Yakovlev, *Phys. Rev. D* **75**, 103004 (2007).
- [23] D. A. Baiko, P. Haensel, and D. G. Yakovlev, *Astron. Astrophys.* **374**, 151 (2001).
- [24] H. Heiselberg and C. J. Pethick, *Phys. Rev. D* **48**, 2916 (1993).
- [25] L. D. Landau and E. M. Lifshitz, *Physique Statistique* (MIR, Moscow, 1967).
- [26] W. L. Slattery, G. D. Doolen, and H. E. De Witt, *Phys. Rev. A* **26**, 2255 (1982).
- [27] D. A. Baiko, A. Y. Potekhin, and D. G. Yakovlev, *Phys. Rev. E* **64**, 057402 (2001).
- [28] A. Y. Potekhin and G. Chabrier, *Contrib. Plasma Phys.* **50**, 82 (2010).
- [29] W. J. Carr, *Phys. Rev.* **122**, 1437 (1961).
- [30] J. W. Negele and D. Vautherin, *Nucl. Phys. A* **207**, 298 (1973).
- [31] G. F. Bertsch and H. Esbensen, *Ann. Phys. (NY)* **209**, 327 (1991).
- [32] J. Wambach, T. L. Ainsworth, and D. Pines, *Nucl. Phys. A* **555**, 128 (1993).
- [33] C. Shen, U. Lombardo, P. Schuck, W. Zuo, and N. Sandulescu, *Phys. Rev. C* **67**, 061302 (2003).
- [34] N. Sandulescu, L. S. Geng, H. Toki, and G. C. Hillhouse, *Phys. Rev. C* **68**, 054323 (2003).
- [35] A. Y. Potekhin, G. Chabrier, and D.G. Yakovlev, *Astron. Astrophys.* **323**, 415 (1997).
- [36] K. P. Levenfish and D. G. Yakovlev, *Astron. Rep.* **38**, 247 (1994).
- [37] D. G. Yakovlev and P. Haensel, *Astron. Astrophys.* **407**, 259 (2003).
- [38] N. Itoh, Y. Kohyama, N. Matsumoto, and M. Seki, *Astrophys. J.* **285**, 758 (1984).